

# Investigation of microwave transitions and nonlinear magneto-optical rotation in anti-relaxation-coated cells

D. Budker,<sup>1,2,y</sup> L. Hollberg,<sup>3</sup> D. F. Kimball,<sup>1</sup> J. Kitching,<sup>3,z</sup> S. Pustelny,<sup>4</sup> and V. V. Yashchuk<sup>5</sup>

<sup>1</sup>Department of Physics, University of California at Berkeley, Berkeley, California 94720-7300

<sup>2</sup>Nuclear Science Division, Lawrence Berkeley National Laboratory, Berkeley, California 94720

<sup>3</sup>National Institute of Standards and Technology, 325 S. Broadway, Boulder, CO 80305-3322

<sup>4</sup>Instytut Fizyki im. M. Smoluchowskiego, Uniwersytet Jagielloński, Reymonta 4, 30-059 Kraków, Poland

<sup>5</sup>Advanced Light Source Division, Lawrence Berkeley National Laboratory, Berkeley CA 94720

(Dated: January 7, 2022)

Using laser optical pumping, widths and frequency shifts are determined for microwave transitions between ground-state hyperfine components of  $^{85}\text{Rb}$  and  $^{87}\text{Rb}$  atoms contained in vapor cells with alkane anti-relaxation coatings. The results are compared with data on Zeeman relaxation obtained in nonlinear magneto-optical rotation (NMOR) experiments, a comparison important for quantitative understanding of spin-relaxation mechanisms in coated cells. By comparing cells manufactured over a forty-year period we demonstrate the long-term stability of coated cells, an important property for atomic clocks and magnetometers.

PACS numbers: 32.30.Bv, 32.70.Jz, 32.80.Bx, 95.55.Sh

## I. INTRODUCTION

Alkali metal vapor cells with paraffin anti-relaxation coatings, first introduced by H. G. Robinson et al. in the 1950's [1] and subsequently studied in great detail by M. A. Bouchiat et al. [2, 3] and other authors (see, for example, Ref. [4] and references therein), are presently at the heart of some of the most sensitive optical-pumping magnetometers [5]. Recently, paraffin-coated cells have also been used in investigations of nonlinear-optics such as nonlinear magneto- and electro-optical effects (see Refs. [6, 7] for detailed reviews). Using coated cells, Zeeman and nonlinear-optical resonance widths of less than 1 Hz and microwave resonance widths of several hertz have been achieved. Although the use of paraffin-coated cells in atomic clocks has also been extensively investigated (see, for example, Refs. [8, 9, 10]), up until now such cells have not been commonly used in commercial clocks despite of their potential advantages, including excellent short-term stability and the sensitivity of the resonance frequency to temperature variations comparable to that of buffer-gas cells (when the gas composition in the case of buffer-gas cells is chosen to minimize the temperature dependence).

The ongoing work aimed at developing highly miniaturized atomic frequency references [11, 12] and magnetometers has created renewed interest in wall coatings. These devices will likely take advantage of miniature atomic vapor cells with physical dimensions on the order of 1 mm or smaller [13]. Because of the larger surface-to-volume ratio, atoms confined in such a small cell spend a

larger fraction of their time interacting with the cell wall than they would in a larger cell. Therefore, linewidth broadening and frequency shifts associated with the cell walls can significantly affect the performance of the frequency reference even when a buffer gas of moderate pressure is used. Thus the quality and efficiency of coatings applied to the walls of such small cells is an important factor in determining the feasibility of highly miniaturized frequency references, particularly those with cell volumes significantly below 1 mm<sup>3</sup>.

Collisions of alkali atoms with cell walls can affect the atomic state in a number of ways. In addition to optical resonance broadening, the atomic ground states can undergo Zeeman and hyperfine decoherence and population transfer. Typically, the hyperfine decoherence rate is found to be about one order of magnitude larger than the Zeeman decoherence rate [9, 14]. For atomic frequency references, the properties of the atomic transition between hyperfine levels determine the short-term stability, while for most magnetometers, transitions between Zeeman levels within a single hyperfine level are important. Thus, investigation of a comparison between different wall-relaxation effects, particularly a comparison of Zeeman and hyperfine decoherence, is of interest both from the viewpoint of understanding the basic physics and with regard to practical applications.

In this paper, we present measurements of intrinsic linewidths and shifts performed with several alkane-coated alkali-vapor cells manufactured in different laboratories over a period of about 40 years. We compare the results to those of the nonlinear magneto-optical rotation (NMOR) [6] experiments, and draw conclusions pertaining to the applications of the coated cells to atomic clocks. Specifically, we find that wall coatings can remain effective for at least several decades after the cell is fabricated, and that for high-quality alkane coatings, neither the molecular weight distribution of the alkane chains nor the method by which the wall coating is de-

This work is a partial contribution of NIST, an agency of the U.S. Government, and is not subject to copyright.

<sup>y</sup>Electronic address: budker@socrates.berkeley.edu

<sup>z</sup>Electronic address: kitching@boulder.nist.gov

posited has much bearing on the effectiveness of the coating. In addition, the NMR linewidth is found to be up to ten times smaller than the hyperfine coherence linewidth when the two are measured in the same cell at similar temperatures. This can be explained by the way in which electron-spin randomization contributes to the decoherence in each of these cases.

## II. THE CELLS

The anti-relaxation-coated buter-gas-free cells used in the present work are listed in Table I. The inner-wall coating of each of these spherical cells was an alkane (general chemical formula  $C_nH_{2n+2}$ ). None of these cells were "re-cured" or heat treated before testing (a procedure that may be used, if necessary, to reduce the relaxation due to alkali metal that has collected on the coated walls).

The cell identified in Table I as G1b, containing a natural mixture of Rb isotopes, was manufactured at Berkeley around 1964 for the Ph.D. thesis work of H. M. Gibbs. (The Thesis [19] gives a detailed description of the cell manufacturing process.) The coating material is Parafint, which consists of alkane chains with a wide range of molecular weights. The coating was applied by melting Parafint wax and running it over the cell surface. This cell has obvious Rb crystalline deposits on the wall and there are several glass tubulations on the spherical surface (i.e., imperfections that originate from glass tubes that were attached to the cell during the manufacturing process). Regions of the cell have heavy pooling of wax and the coating thickness is very non-uniform.

The  $^{85}\text{Rb}$  cell referred to as Ale-10 was made by E. B. Alexandrov and M. V. Balabas according to the procedure described, for example, in Ref. [20]. The material of the coating is a mixture of alkane chains of different length ( $n \approx 50$ ) fractionated from polyethylene at 220°C. The coating was applied by vapor deposition, where a piece of the paraffin was placed in a side-arm and the whole cell was heated to fill it with the paraffin vapor, and then cooled. The resulting coating has estimated thickness of  $\approx 10 \text{ nm}$ , and can be barely seen by eye.

The  $^{87}\text{Rb}$  cells referred to as TT11 and H2 were made by H. G. Robinson [21]. The material of the coating is tetracontane ( $n=40$ ) distilled at about 200°C. The purified tetracontane wax was evaporatively coated onto the cell surface from a hot needle. The resulting coating is thin (and so not visible by eye) and has a melting temperature of  $\approx 80^\circ\text{C}$ .

Each cell with the exception of G1b was made with an uncoated stem containing rubidium metal (see also Section VI).

## III. MICROWAVE-TRANSITION MEASUREMENTS

A schematic of the apparatus is shown in Fig.1. We used a distributed-Bragg-reflector (DBR) diode laser [16] with a measured linewidth of  $\approx 2 \text{ MHz}$ , whose frequency was tuned near the Rb D1 resonance ( $\lambda = 795 \text{ nm}$ ). The light beam passes through a variable attenuator, an optical isolator used to avoid optical feedback into the laser, and then a linear polarizer. It is then directed through a vapor cell (at room temperature) enclosed in a single-layer cylindrical magnetic shield. The laser beam diameter at the location of the cell is  $\approx 7 \text{ mm}$ . The intensity of the transmitted light is detected with a photodiode. A dc magnetic field is applied to the cell parallel to the direction of light propagation by passing current through a coil wound on the surface of a cylindrical acrylic insert (not shown) that fits into the magnetic shield. A microwave field is applied with a single-wire loop terminating a coaxial cable. The microwave synthesizer is referenced to a hydrogen maser ( $\Delta = 2 \cdot 10^{-3} \text{ s}^{-2}$ , where  $\Delta$  is measured in seconds).

For one cell (TT11 [38], see Table I), a slightly different apparatus was used. The magnetic shield consisted of two layers, and a low-Q (of several thousand) cylindrical microwave cavity operating in the  $\text{TE}_{011}$  mode was employed instead of the wire loop. In this apparatus, it was possible to heat the cell while keeping the stem at a lower temperature. This was useful for evaluating the effect of the temperature on the widths and shifts of the microwave transition.

In the experiment, the laser frequency was tuned to a particular location on the optical absorption profile, and the microwave frequency was swept around the nominal frequency of the field-free separation of the ground-state hyperfine components of  $^{85}\text{Rb}$ : 3;035;732;440 Hz [17] or  $^{87}\text{Rb}$ : 6;834;682;610.9 Hz [18], while the transmitted light intensity was recorded. An applied dc magnetic field gave rise to the splittings as shown in the microwave spectra of Figs. 2 and 3.

## IV. NONLINEAR MAGNETO-OPTICAL MEASUREMENTS OF ZEEMAN RELAXATION

For all cells except TT11, in addition to studying microwave transitions, we also measured Zeeman relaxation rates using nonlinear magneto-optical rotation. The general idea of the method is the following (see the review [6] for a detailed discussion). The interaction of the atoms with a near-resonant laser field results in polarization of the atomic medium. The induced polarization evolves in the presence of a magnetic field; the resulting change of the medium's polarization is detected by measuring optical rotation of the linearly polarized light (which, in this case, plays the part of both the pump and the probe). In this work, we used a version of the NMR technique in which the frequency of the laser is modulated and optical

TABLE I: Vapor cells used for the measurements and the experimentally determined values of microwave linewidths ( $\gamma_{\text{exp}}$ ) and shifts.  $T$  – the temperature of the cell (which was higher than that for the stem for some of the measurements).  $n$  – the total number density of Rb vapor. The quantity  $\gamma_{\text{se}}$  is the estimated average phase shift per wall collision. The uncertainty in  $\gamma_{\text{se}}$  includes an estimate of the effect of non-ideal cell shape. For  $^{87}\text{Rb}$ , the phase shift  $\gamma_{\text{se}}^0$  scaled to  $^{85}\text{Rb}$  (see text) is also given. The last two columns list the deduced contributions to the microwave linewidths from the spin-exchange collisions and the adiabatic collisions, respectively (see text).

Cell	Year made	Ref.	Diam. (cm)	$T$ (°C)	$n$ ( $\text{cm}^{-3}$ )	Isotope	$\gamma_{\text{exp}}/2$ (Hz)	Shift (Hz)	$\gamma_{\text{se}}/2$ (rad)	$\gamma_{\text{se}}^0/2$ (rad)	$\gamma_{\text{se}}/2$ (Hz)	$\gamma_{\text{ad}}/2$ (Hz)
Ale-10	1997	[20]	10	25	$8 \cdot 10^{10}$	$^{85}\text{Rb}$	8.7(5)	-24(4)	0.037(7)		1.3	2
Gib	1964	[19]	10	25	$8 \cdot 10^{10}$	$^{85}\text{Rb}$	11(2)	-14(4)	0.022(6)		1.3	0.6
						$^{87}\text{Rb}$	16(4)	-42(2)	0.065(6)	0.029(3)	1.2	5
H2	1985	[21]	3.5	21	$7 \cdot 10^{10}$	$^{87}\text{Rb}$	22(3)	-93(1)	0.050(5)	0.022(2)	1.2	9
TT11	1985	[21]	3.4	22	$6.5 \cdot 10^{10}$	$^{87}\text{Rb}$	23(2)	-80(1)	0.043(4)	0.019(2)	1.0	7
				42	$1.4 \cdot 10^{10}$		17.5(10)				2.2	
				43	$3.4 \cdot 10^{10}$		21.5(10)	-70.5(3)	0.036(4)	0.016(2)	5.2	5

TABLE II: Experimentally determined values for FM NMR linewidths.  $T$  – the temperature of the cell (the stem and the cell body are at the same temperature).  $n$  – the total number density of Rb vapor.  $\gamma_{\text{se}}^{\text{NMR}}$  – calculated spin-exchange contribution to the NMR linewidth. The last column lists the deduced contributions to the microwave linewidths from electron-spin-randomization collisions (see text).

Cell	$T$ (°C)	$n$ ( $\text{cm}^{-3}$ )	Isotope	$\gamma_{\text{exp}}^{\text{NMR}} = (2 \cdot \gamma)$ (Hz)	$\gamma_{\text{se}}^{\text{NMR}} = (2 \cdot \gamma)$ (Hz)	$\gamma_{\text{er}} = (2 \cdot \gamma)$ (Hz)
Ale-10	19	$4 \cdot 10^{10}$	$^{85}\text{Rb}$	0.7(1)	0.15	3
	25	$6 \cdot 10^{10}$	$^{85}\text{Rb}$	1.2(1)	0.24	5
Gib	21	$4 \cdot 10^{10}$	$^{85}\text{Rb}$	2.9(1)	0.15	13
			$^{87}\text{Rb}$	2.9(1)	0.24	9
H2	21	$4 \cdot 10^{10}$	$^{87}\text{Rb}$	3.5(1)	0.24	11

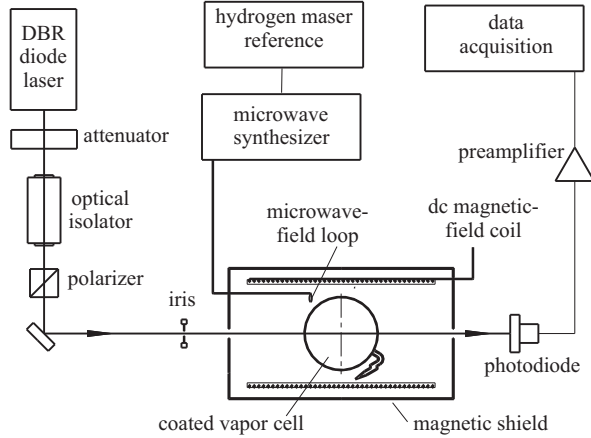


FIG. 1: Experimental setup for measuring microwave transitions.

rotation varying at the modulation frequency is detected (FM NMR [22, 23, 24]; Fig. 4).

The vapor cell under study was placed inside a multi-layer magnetic shielding system (not shown) equipped with coils for compensating residual magnetic fields and gradients and for applying well controlled fields to the cell. The time-dependent optical rotation was detected with a balanced polarimeter after the vapor cell. In this

work, the laser was tuned to the Rb D1 line; the laser beam diameter was 2 mm, and the light power was  $< 15 \text{ W}$ . A static magnetic field was applied along the light propagation direction. Narrow resonances in modulation frequency appear in the synchronously detected optical-rotation signal when the frequency is equal to twice the Larmor frequency (Fig. 5). The factor of two is related to the two-fold spatial symmetry of the induced atomic alignment. The widths of the resonances are determined by the ground-state Zeeman relaxation rate.

An advantage of the FM NMR technique for measuring the Zeeman relaxation rate is that when a bias field is applied (as in the present case), the resonance curves are, to first order, insensitive to small transverse magnetic fields; this eliminates a possible source of systematic error.

## V. PROCEDURE, RESULTS AND DISCUSSION

The total electronic angular momentum in the ground electronic state of rubidium is  $J = 1/2$ . For  $^{85}\text{Rb}$ , the nuclear spin is  $I = 5/2$ . In a low dc magnetic field where nonlinear Zeeman shifts resulting from decoupling of hyperfine structure can be neglected, one generally expects to see 11 distinct resonance hyperfine transition frequencies between various linear-Zeeman-split sublevels of the

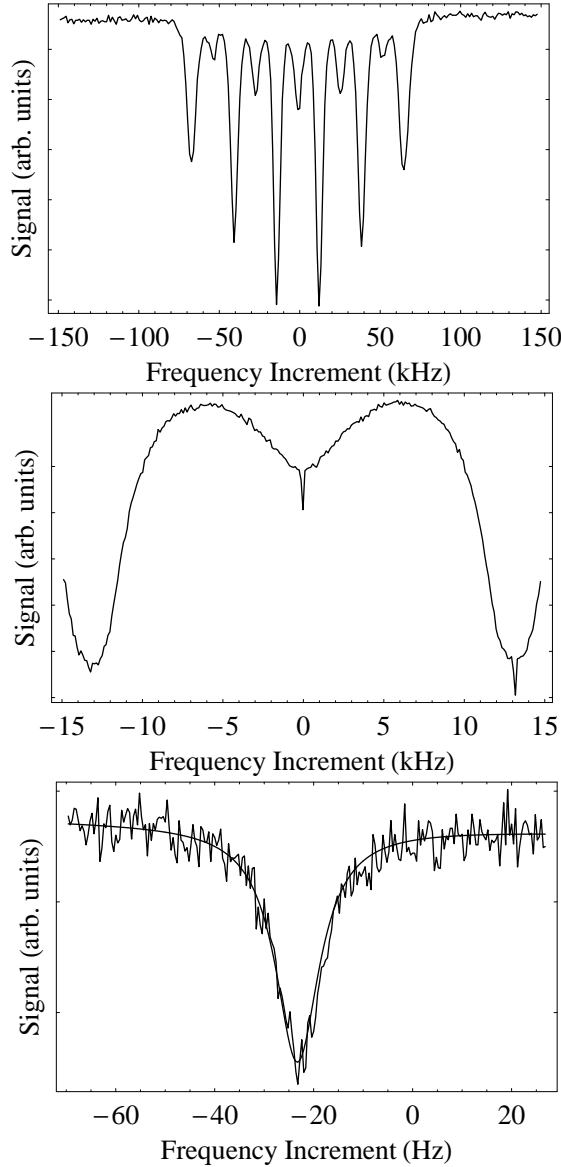


FIG. 2: Examples of the microwave spectra recorded with the Ale-10  $^{85}\text{Rb}$  cell (see Table I). The signal corresponds to the intensity of the laser light transmitted through the cell. The common parameters for the three scans are: dc magnetic field = 29 mG, linear light polarization, laser tuned to the center of the  $F = 3 \rightarrow F^0$  transition, total scan rate (saw-tooth sweep) = 0.02 Hz. Each plot represents an average of approximately five scans. Upper and middle plots: input light power 0.25 W; lower plot: input light power 13 W, microwave power reduced by a factor 63. The lower plot also shows a fit by a Lorentzian superimposed on a linear background. The Lorentzian linewidth (FWHM) is 10.9(3) Hz, slightly larger than the "intrinsic" width of about 8.7 Hz (Table I) due to residual light broadening (see text).

upper and lower ground-state hyperfine levels. (For  $^{87}\text{Rb}$ , an atom with  $I = 3/2$ , there are 7 transition frequencies.) The experimental observation of this is shown in the upper plot of Fig. 2). The relative intensities of various

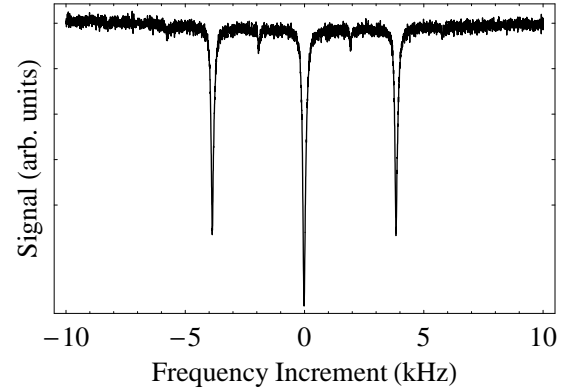


FIG. 3: An example of a microwave spectrum recorded with the T11  $^{87}\text{Rb}$  cell (see Table I). The parameters for the scan are: dc magnetic field = 2.7 mG, linear light polarization, laser tuned to the center of the  $F = 2 \rightarrow F^0$  transition, total scan rate (saw-tooth sweep) = 0.2 Hz. The plot represents a single scan. Input light power = 6 W. The comparison of this plot with the middle plot in Fig. 2 illustrates the advantages of using a TE<sub>011</sub> microwave cavity as opposed to a current loop: almost complete suppression of the broad pedestal and the  $M_F \neq 0$  microwave transitions.

components depend on the power, polarization, and tuning of the pump light, the geometry and orientation of the microwave loop, and the microwave power. Under typical conditions in this experiment, the peaks of the resonances correspond to an increase in absorption by several percent (the optical depth on resonance of the room-temperature cells is of order unity).

The width of the peaks on the upper plot in Fig. 2 is about 4 kHz (FWHM) and is dominated by the Doppler width of the microwave transition. There is also a significant contribution due to the phase variation of the microwave field over the cell volume resulting from the use of a simple loop for generation of the microwave field. A zoom with higher frequency resolution (the middle plot in Fig. 2) reveals additional sharp features superimposed on top of the Doppler-broadened lines. These are the Dicke-narrowed lines [9, 25] of primary interest in the present work.

While all the sharp features are of comparable widths, in the following we concentrate on the central resonance corresponding to the "clock transition" between the  $M = 0$  Zeeman components (the 0-0 transition), which is to first order insensitive to dc magnetic fields and gradients. An example of a high-resolution recording of the narrow feature is shown in the lower plot in Fig. 2. The line shape is well described by a Lorentzian as seen from the fitting curve also shown in the plot.

We have measured the widths and shifts of the central narrow resonance for each of the cells. In order to eliminate the effects of power broadening and shifts, we performed double extrapolation of the widths and central frequencies of the resonances to zero optical and microwave power, using their observed linear dependence

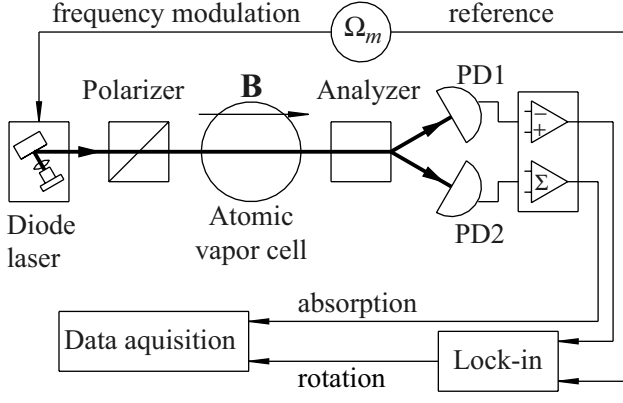


FIG. 4: Simplified schematic of the experimental setup for measuring Zeeman relaxation rate with the FM NMOR technique [22, 23, 24].

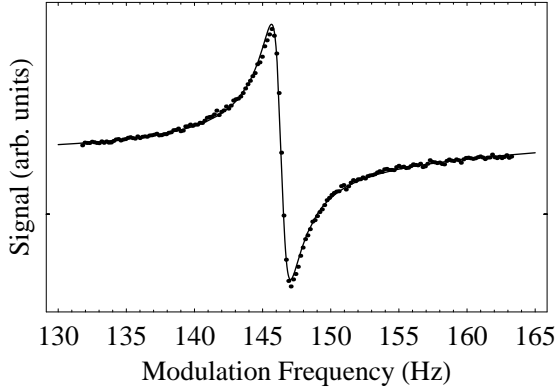


FIG. 5: An example of the FM NMOR data (the lock-in detector output, see Fig. 4) taken with the Ale-10 cell. The central frequency of the laser is tuned 400 MHz lower than the center of the  $F = 3 \rightarrow F^0$  absorption peak of the D1 line (this point corresponds to a maximum of the FM NMOR signal). The laser frequency is modulated with an amplitude of 20 MHz. A bias magnetic field of 156 G is applied along the light-propagation direction. The data are shown along with a fit by a dispersive Lorentzian (see Ref. [24]). The width of the resonance corresponds to  $\Delta \nu_{\text{exp}}^{\text{NMOR}} = 2.07$  Hz, the narrowest magneto-optical resonance width observed with alkali atoms to date.

on power at low powers. (The effects of light broadening can also be minimized by judicious choice of light tuning; for example, the high-frequency slope of the  $^{85}\text{Rb}$   $F = 3 \rightarrow F^0$  optical transition provides relatively large signals with greatly reduced light broadening. The signal deteriorates on the low-frequency slope, presumably because Zeeman optical pumping dominates over hyperfine pumping. Similar "tricks" are also used in optical pumping magnetometry [27] and in NMOR [28, 29].) The results, which were found to be independent of laser tuning and polarization, are summarized in Table I. For  $^{85}\text{Rb}$ , uncertainties in the shifts include both the errors of the present measurement and 3 Hz uncertainty in the knowl-

edge of the absolute transition frequency for free atoms [26]; for  $^{87}\text{Rb}$ , the latter uncertainty is negligible [18].

An example of the data taken with the microwave cavity is shown in Fig. 3. The  $\text{TE}_{011}$  cavity has important advantages over a simple loop, as can be seen from the comparison of Fig. 3 with the middle plot in Fig. 2. In particular, strong suppression of the broad pedestal and the  $M_F \neq 0$  microwave transitions is apparent. (In Ref. [10], microwave transition lineshapes obtained using  $\text{TE}_{011}$  and  $\text{TE}_{111}$  cavities were compared to each other. Narrow lines appeared only when the  $\text{TE}_{011}$  cavity was used. Ref. [10] also contains references to calculations of the lineshape in the regime in which the dimensions of the cell are comparable with the wavelength, and, correspondingly, with the microwave cavity mode size.)

As an additional cross-check of the results given in Table I, a set of room temperature data for the H2 cell was also taken using the 780 nm D2 resonance (a different diode laser system was used for this measurement). The results, the intrinsic width of 20.3(9) Hz and shift of 89.5(11) Hz, are consistent with the data obtained with D1 resonance (see Table I), as expected.

The data taken at different temperatures in the TT11 cell provide some insight into the adsorption process of the alkali atoms onto the walls. The adsorption time of the atom on the wall, under simplifying assumptions such as a uniform adsorption energy on all sites on the surface, is usually assumed to be [30]

$$\tau_a = \tau_0 e^{E_a/kT}; \quad (1)$$

where  $\tau_0$  is the period of vibration of the adsorbed atom in the wall potential,  $E_a$  is the adsorption energy,  $k$  is the Boltzmann constant and  $T$  is the absolute temperature. At higher temperatures, therefore, an atom spends less time on the wall and should experience a smaller frequency shift and broadening. The frequency shift (discussed in the following section) in particular should be reduced by a factor equal to the fractional change in adsorption time due to the change in cell temperature:

$$\frac{d}{dT} = \frac{E_a}{kT} \frac{dT}{T}; \quad (2)$$

For the TT11 cell, the frequency shift measured at two temperatures allows one to calculate (under the assumptions of Eq. (1)) the adsorption energy, giving  $E_a = 0.06$  eV. This is consistent with previous values found in similar cells but smaller than the 0.1 eV reported by some researchers (see Ref. [31] and references therein).

In interpreting the observed microwave frequency shifts we have assumed that these shifts originate in collisions of rubidium atoms with the cell walls because the cells studied here are nominally free from buffer gas. However, due to high mobility of helium atoms in glass, it is possible that atmospheric helium has diffused into the cells through the glass (particularly in the case of the oldest G1b cell). Assuming that the helium inside the cells is in equilibrium with that in the atmosphere (for

which the partial He concentration is  $5.2 \times 10^{-6}$ ) and using the literature data (e.g., Ref. [15]) for the frequency shifts of the rubidium 0-0 microwave transitions, we find that the microwave resonance is shifted by +1.3 Hz and +2.9 Hz for  $^{85}\text{Rb}$  and  $^{87}\text{Rb}$ , respectively. Since these shifts are relatively small, and since we do not know the actual pressure of helium in the cells, we ignore these shifts in the rest of the paper, noting them as a possible source of a small systematic error. Broadening due to collisions with helium is negligibly small.

The procedure for obtaining the Zeeman relaxation data is described in Refs. [22, 24]. Care was exercised to minimize the possible contributions to resonance linewidths due to magnetic-field gradients (which were compensated to a level  $< 1 \text{ G/cm}$ ). The contribution of gradient broadening to the FM-NMR linewidth (upon compensation of the gradients) is found to be negligible at the level of present uncertainties [32]. Similar to the procedure used for the microwave transitions, the observed resonance widths (see Fig. 5) were extrapolated to zero light power.

Atomic number densities listed in Tables I and II were determined by fitting linear absorption spectra taken at low light power ( $< 1 \text{ W}$ ).

## V I. I N T E R P R E T A T I O N

There are several known relaxation mechanisms at work in the vapor cells studied here, including spin-exchange relaxation, loss of polarized atoms due to collisions with uncoated surfaces (primarily in the cell's stem), and relaxation due to collisions with the wall coating.

The contribution of spin-exchange relaxation to the microwave width can be estimated using the formulae given in Refs. [33, 34]. When only one isotope with nuclear spin  $I$  is present in the cell, the spin-exchange contribution to the linewidth of the 0-0 microwave transition is given by

$$\frac{\gamma_{se}}{2} = \frac{R(I)n\bar{v}_{rel\ se}}{2}; \quad (3)$$

where  $\gamma_{se}$  is the spin-exchange-collision cross-section ( $\gamma_{se} = 2 \times 10^4 \text{ cm}^2$  for all cases relevant here [34]),  $n$  is the atomic number density,

$$\bar{v}_{rel} = \frac{p}{8kT} = \frac{p}{m_{red}} \quad (4)$$

is the average relative speed, and  $m_{red}$  is the reduced mass of the colliding atoms, and

$$R(I) = \frac{6I + 1}{8I + 4} \quad (5)$$

is the so-called nuclear slow-down factor (see Refs. [33, 34]) for the 0-0 transition. For the GIB cell, where two isotopes are present, the considerations are similar. The values of the contribution of the spin-exchange collisions

to the microwave linewidths deduced from the measured number density are listed in the next-to-last column of Table I. In all cases, this contribution is less than 25% of the overall observed linewidth  $\gamma_{exp}$ .

The relaxation due to the stem can be estimated from the geometry (except for the GIB cell which does not have a stem, whose deposits of solid rubidium are apparently covered with paraffin), and is found to contribute to the microwave linewidth less than a fraction of a hertz in the case of the ALE-10 cell and less than 1 Hz in the case of the T11 and H2 cells. Effects related to the cell stems therefore contribute to the hyperfine decoherence at a level somewhat less than the measurement errors given in Table I. We ignore this contribution in the following discussion.

Collisions of alkali atoms with the wall coating can be separated into three categories. The most "gentle" or adiabatic collisions, while causing hyperfine transition frequency shift and decoherence (as discussed below), generally do not result in population transfer or Zeeman decoherence. The stronger collisions, for example, collisions with paramagnetic impurities or "dangling bonds," randomize the electron spin. However, they do not affect the nuclear spin, so a polarized atom retains a certain degree of polarization after the collision. Finally, an atom can be absorbed into the coating for a sufficiently long time that all polarization is destroyed. First, we analyze the contribution of the adiabatic collisions.

While the adiabatic collisions do not cause atoms to jump between quantum states, the interaction with the wall during a collision causes a phase shift between hyperfine states [30]. The hyperfine transition frequency shift due to this phase shift can be estimated as follows. Consider an atom in the cell that we will track for a time much longer than the typical interval between its wall collisions. The distance travelled by the atom (along some complicated reticulated trajectory) is  $\bar{v}t$ , where

$$\bar{v} = \frac{p}{8kT} = \frac{p}{M} \quad (6)$$

is the mean speed and  $M$  is the mass of the atom. The next question is: how many times did this atom collide with the wall? The answer for a spherical cell (for which the mean distance between wall collisions assuming the usual cosine angular distribution of atoms bouncing off the wall is  $4R/3$ ) is

$$\frac{\bar{v}}{4R/3} = \frac{1}{t_c}; \quad (7)$$

where  $t_c$  is the characteristic time between wall collisions. If the phase shift per collision is  $\phi$ , the overall phase increment in time  $t$  is

$$\frac{\bar{v}}{4R/3} t \phi; \quad (8)$$

On the other hand, the phase increment is also equal to

$$2\pi \nu t; \quad (9)$$

TABLE III: Linewidth budget for the microwave transitions.  $\Delta_a = (2)$  and  $\Delta_{er} = (2)$  are the deduced contributions to the microwave linewidth from adiabatic and electron-randomization collisions (from Tables I and II), respectively. The last two columns list the total expected width based on the sum of these deduced contributions and the experimentally observed microwave linewidths (from Table I).

Cell	Isotope	$\Delta_a = (2)$ (Hz)	$\Delta_{er} = (2)$ (Hz)	Total (Hz)	$\Delta_{exp} = (2)$ (Hz)
Al-10	$^{85}\text{Rb}$	2	5	7	8.7(5)
Gib	$^{85}\text{Rb}$	0.6	13	14	11(2)
	$^{87}\text{Rb}$	5	9	14	16(4)
H2	$^{87}\text{Rb}$	9	11	20	22(3)

where  $\Delta$  is the frequency shift. Equating (8) and (9), and cancelling  $\Delta$ , we get

$$\Delta = \frac{3\overline{\nu}}{2} \frac{1}{4R} : \quad (10)$$

The values of the phase shift  $\Delta$  for various cells, experimental conditions, and Rb isotopes, deduced from the experimental values of the microwave transition frequency shifts using Eq. (10), are listed in Table I. The results are consistent with the available earlier data for Rb in alkane-coated cells (Ref. [9] and references therein) within the spread between different cells under similar conditions and with the same Rb isotope.

In order to compare the coating properties for cells containing different isotopes, one can scale the phase shift to one and the same isotope (e.g.,  $^{85}\text{Rb}$ ) using the expected proportionality of the phase shift and the hyperfine transition frequency [39]. The scaled values ( $\Delta^0$ ) for the  $^{87}\text{Rb}$  data are listed in Table I. The results indicate that all the different coatings studied in this work produce roughly the same phase shifts in wall collisions. We also note that the phase shifts per collision measured here in Rb are roughly consistent with those measured for Cs on paraffin coatings ( $\Delta = 0.09(1)$  rad [30]), when scaled to the corresponding hyperfine frequency.

Because of the statistical character of the collisions, there is a spread in the amount of phase shift acquired by the atoms, which contributes to the resonance width [30, 35] (a derivation of the broadening and shift due to this mechanism is given in the Appendix):

$$\frac{\Delta}{2} = \frac{1}{t_c} : \quad (11)$$

For the parameters and the frequency shifts measured in the present experiment, these contributions to the width comprise from  $\Delta_a = (2)$  0.6 Hz to 10 Hz. As seen from Table I, the sums of  $\Delta_a$  and  $\Delta_{se}$  are insufficient to explain the observed overall intrinsic widths  $\Delta_{exp}$  in any of the cases.

A possible contribution to the linewidth that may explain this is from electron-spin randomizing collisions with the wall or, possibly, gaseous impurities other than helium [2]. The magnitude of this contribution to the width of the microwave transitions can be estimated from the assumption that the measured NMR linewidths

( $\Delta_{exp}^{NMR}$ ) are also dominated by electron-spin randomization collisions [36]. The measured NMR linewidths are broader than what is expected given the known spin-exchange cross-sections (see Table II). The relaxation rate of the 0-0 microwave coherence due to spin randomization should be 3/4 of the electron randomization rate [34], while the intrinsic NMR linewidth due to electron-spin randomization is smaller, due to the nuclear slowdown effect (see, for example, Ref. [34]), and is calculated to be 1/3 of the spin-randomization rate for  $^{85}\text{Rb}$  and 1/2 for  $^{87}\text{Rb}$  [36].

Using this information, the contribution of the electron-spin randomization collisions to the microwave linewidth can be estimated ( $\Delta_{er}$ , Table II). For example, for the Al-10 cell at 25 C, assuming that the Zeeman relaxation is dominated by spin-randomization collisions, we have

$$\frac{\Delta_{er}}{2} = 2 \quad (1.2 \text{ Hz}) \quad 3 \frac{3}{4} = 5 \text{ Hz} : \quad (12)$$

In expression (12), the factor of two accounts for the relation between the relaxation rate for the 0-0 coherence and the Lorentzian width of the microwave transition. (Under the conditions of our experiments, in which linearly polarized low-intensity light is used, the effect of spin-exchange collisions is nearly identical to that of electron-randomization collisions [34], and we do not separate spin exchange from the additional electron-randomization processes in this estimate and those presented in Tables II and III.) Adding up all the contributions and estimating the associated uncertainties, we find that for the Al-10 cell we can account for about 7(1) Hz out of the observed 8.7(5) Hz, which is satisfactory, particularly, in view of a number of simplifying assumptions in our model (for example, the assumption that the dispersion of  $\Delta$  is equal to  $\Delta^2$  in the adiabatic collisions, see Appendix). The microwave linewidth budgets for the cells where both the microwave and NMR data are available are summarized in Table III.

The fact that both Rb isotopes are simultaneously present in the Gib cell allows a check of our model for consistency, and provides further evidence that the dispersion of phase shifts in adiabatic collisions is not the dominant source of the microwave linewidth. For the values of  $\Delta$  (Table I) for the two isotopes extracted from the measured frequency shifts using Eq. (10), Eq. (11) pre-

dicts about an order of magnitude larger contribution to the width from phase-shift dispersion in adiabatic collisions for  $^{87}\text{Rb}$  compared to that for  $^{85}\text{Rb}$ . This is clearly inconsistent with a relatively small difference in the width observed experimentally, but does correspond to the prediction of our model.

So far, we have considered adiabatic and electron-spin randomization collisions. Collisions that completely depolarize atoms would also contribute to both the hyperfine and Zeeman relaxation. However, if one assumes that relaxation is dominated by collisions of this type rather than electron-randomization collisions, carrying out an analysis similar to the one above, one does not achieve satisfactory agreement between the microwave and NMR linewidths.

The present experimental data for the widths and shifts of the microwave transitions appears inconsistent with a hypothesis that the linewidth is dominated by dispersion of the phase shifts in adiabatic wall collisions. On the other hand, comparing the microwave data and the Zeeman relaxation data measured with nonlinear magneto-optical rotation, we have proposed that the dominant source of the linewidth is electron-spin randomizing collisions. This hypothesis consistently accounts for the linewidth-budget deficits for both microwave transitions and NMR resonances. The rate of the electron-randomization collisions necessary to explain the observed microwave and NMR linewidths is too large to be accounted for by spin-exchange collisions (Tables I and II). Thus it is necessary to assume electron randomization processes occurring either in collisions of the alkali atoms with cell walls or, possibly, in collisions with gaseous impurities. These two scenarios may be distinguished by comparing relaxation rates for otherwise similar cells having vastly different diameters.

It is interesting to compare the present results with those of Ref. [15]. In that work, the rates of the hyperfine-coherence and population relaxation in wall collisions in a Parafilm-coated cell were measured, and the latter was found to be an order of magnitude lower than the former. In the present experiment, since we have found that electron-randomization collisions dominate relaxation at room temperature, one would expect that the two rates should be similar. This apparent contradiction may be attributable to an important difference of the experimental procedure of Ref. [15] compared to that of this work: namely that the data were obtained in the limit of zero rubidium density in the cell (which was achieved by maintaining the stem at a temperature lower than that of the cell walls). This may suggest that the electron randomization in our case is due to a modification of the coating surface due to the presence of rubidium atoms. These issues will be addressed in future work.

## V II. CONCLUSION

It appears that the vapor-cell coatings studied in this work, manufactured using three rather different technologies, all show comparable performance in terms of the parameters (linewidth and shift) relevant to their use in magnetometers and atomic clocks. Moreover, the fact that a cell (Gib) manufactured 40 years ago shows comparable performance to that of more recently manufactured cells is evidence of the stability of the coating properties [40] and suitability of such cells for extremely long term measurements, for example, as frequency-reference and magnetic-sensor elements for deep-space missions.

The durability of the wall coatings and the lack of dependence of the coating properties on the exact molecular-weight composition and the method of coating deposition are encouraging with regard to the application of such coatings to miniature atomic frequency references. Wall coatings might play an important role in improving the performance of compact atomic clocks if a way of integrating the application of the coating with the cell fabrication process is found. This integration will likely be an important future step in the development of atomic clocks based on submillimeter alkali-atom vapor cells.

This work was initiated and inspired by H. G. Robinson, who has contributed greatly to its realization. The authors are grateful to D. English, S. M. Rochester, and J. E. Stalnaker for useful discussions and help with data analysis, to S. N. Evans for his help in understanding the statistics underlying collisional broadening and shift, and to H. Shugart, E. B. Alexandrov, M. V. Balabas and Symmetrium, TRC for providing the anti-relaxation-coated cells. This work was supported by the Office of Naval Research, National Science Foundation (NSF), by a CalSpace Minorant, and by the Microsystem Technology Office of the Defence Advanced Research Projects Agency (DARPA). D.B. also acknowledges the support of the Miller Institute for Basic Research in Science.

## V III. APPENDIX

Here we give a derivation of line broadening and shift arising from the collisional phase shifts acquired by atoms.

Suppose a collection of atomic oscillators are all in phase initially, and in the absence of collisions, they all oscillate at a frequency  $\omega_0$ . Let  $\phi$  be the average phase shift per collision, and  $1/\tau_c$  the average collision rate. There are two factors that lead to a dispersion in different atoms' phase shifts acquired after a time  $t - t_c$ . First, there is a statistical distribution of the number of collisions  $n$  experienced by atoms over a time  $t$  which we will assume to be Poissonian:

$$p(n;t) = \frac{e^{-t/\tau_c} (t/\tau_c)^n}{n!}; \quad (13)$$



where  $p(n;t)$  is the probability that an atom experiences  $n$  collisions in time  $t$  [the mean number of collisions corresponding to the distribution (13) is  $\langle n \rangle = t/t_c$ ]. Second, the phase shifts per collision are not the same. We will assume a normal distribution with a mean value  $\langle \phi_j \rangle = 0$  and a dispersion  $\sigma^2$ . (The latter property follows from a distribution of wall-sticking times with a universal binding energy exceeding  $kT$ ; see, for example, Ref. [30].)

Let us consider atoms that have experienced some fixed number of collisions  $n \geq 1$ . Let  $\phi_n$  be the overall phase accumulated by an atom over  $n$  collisions. Because of the normal distribution of phase shifts in individual collisions (resulting in a random walk in phase), we have a Gaussian distribution of accumulated phases:

$$p(\phi_n; n) = \frac{1}{\sqrt{2\pi n \sigma^2}} e^{-\frac{(\phi_n - \langle \phi_n \rangle)^2}{2n \sigma^2}}; \quad (14)$$

where  $\langle \phi_n \rangle$  is the average phase accumulated in  $n$  collisions, and  $n \sigma^2$  is the dispersion.

Taking into account the distributions (13) and (14), the oscillation amplitude averaged over the atomic ensemble is found as a weighted sum of the contributions from individual atoms ( $\propto e^{i(\omega_0 t + \phi_j)}$ ), where  $\phi_j$  is the phase accumulated by this individual atom):

$$A(t) / \sum_{n=0}^{\infty} \frac{e^{-t/t_c} (t/t_c)^n}{n!} \int_{-\infty}^{\infty} \frac{e^{i(\omega_0 t + \phi_n)} e^{-\frac{(\phi_n - \langle \phi_n \rangle)^2}{2n \sigma^2}}}{\sqrt{2\pi n \sigma^2}} d\phi_n \quad (15)$$

$$= e^{i\omega_0 t} e^{-t/t_c} e^{-\frac{1}{2} \frac{t}{t_c} \sigma^2}; \quad (16)$$

where in the last step we have explicitly evaluated the integral and the sum. Next, we use the fact that  $\langle \phi_j \rangle = 0$ , and, expanding the exponential factor to second order in  $\phi_j$ , we obtain

$$A(t) / e^{i(\omega_0 - \omega_c)t} e^{-t/t_c}; \quad (17)$$

which says that the frequency of the oscillation is shifted by  $\omega_c$ , and the amplitude decays at a rate  $1/t_c$ , leading to line broadening. (It is interesting to note that neglecting either one of the random factors { the number of collisions experienced by an atom or the dispersion in phase shift per collision } leads to a two times slower decay rate in either case.) In order to obtain the line width of the absorption resonance, the decay rate of the amplitude has to be multiplied by a factor of two. Therefore, Eq. (17) gives the formulae (10) and (11).

- 
- [1] H. Robinson, E. Ensberg, and H. Dehmelt, *Bull. Am. Phys. Soc.* 3, 9 (1958).
- [2] M. A. Bouchiat, Ph.D. thesis, L'Université de Paris (1964).
- [3] M. A. Bouchiat and J. Brosel, *Phys. Rev.* 147 (1), 41 (1966).
- [4] V. Liberman and R. J. Knize, *Phys. Rev. A* 34 (6), 5115 (1986).
- [5] E. B. Aleksandrov and V. A. Bonch-Bruyevich, *Opt. Eng.* 31 (4), 711 (1992).
- [6] D. Budker, W. Gawlik, D. F. Kimball, S. M. Rochester, V. V. Yashchuk, and A. Weiss, *Rev. Mod. Phys.* 74 (4), 1153 (2002).
- [7] E. B. Aleksandrov, M. Auzinsh, D. Budker, D. F. Kimball, S. M. Rochester, and V. V. Yashchuk, *Dynamical effects in nonlinear magneto-optics of atoms and molecules* (2004), physics/0405049.
- [8] A. Risley, J. Jarvis, S., and J. Vanier, *J. Appl. Phys. (USA)* 51 (9), 4571 (1980).
- [9] H. G. Robinson and C. E. Johnson, *Appl. Phys. Lett.* 40 (9), 771 (1982).
- [10] R. P. Frueholz, C. H. Volk, and J. C. Camargo, *J. Appl. Phys. (USA)* 54 (10), 5613 (1983).
- [11] J. Kitching, S. Knappe, and L. Hollberg, *Appl. Phys. Lett.* 81, 553 (2002).
- [12] Y. Y. Jau, A. B. Post, N. N. Kuzma, A. M. Braun, M. V. Romalis, and W. Happer, *Phys. Rev. Lett.* 92 (11), 110801/1 (2004).
- [13] L. Liew, S. Knappe, J. Moreland, H. G. Robinson, L. Hollberg, and J. Kitching, *Appl. Phys. Lett.* 84 (14), 2694 (2004).
- [14] H. G. Robinson and C. E. Johnson, *IEEE Trans. Instrum. Meas.* IM-32, 198 (1983).
- [15] J. Vanier, J. F. Simard, and J. S. Boulanger, *Phys. Rev. A* 9 (3), 1031 (1974).
- [16] T. Hirata, M. Mameda, M. Suehiro, and H. Hosomatsu, *IEEE J. Quantum Electron.* 27 (6), 1609 (1991).
- [17] M. Tetu, R. Fortin, and J. Y. Savard, *IEEE Trans. Instrum. Meas.* 25, 477 (1976).
- [18] S. Bize, Y. Sortais, M. S. Santos, C. Mandache, A. Clairon, and C. Salomon, *Europhys. Lett.* 45 (5), 558 (1999).
- [19] H. M. Gibbs, Ph.D. thesis, University of California, Berkeley (1965).
- [20] E. B. Aleksandrov, M. V. Balabas, D. Budker, D. English, D. F. Kimball, C. H. Li, and V. V. Yashchuk, *Phys. Rev. A* 66 (4), 042903/1 (2002).
- [21] H. G. Robinson (1985), unpublished.
- [22] D. Budker, D. F. Kimball, V. V. Yashchuk, and M. Zolotarev, *Phys. Rev. A* 65, 055403 (2002).
- [23] V. V. Yashchuk, D. Budker, W. Gawlik, D. F. Kimball,

- Y. P. Malakyan, and S. M. Rochester, *Phys. Rev. Lett.* 90, 253001 (2003).
- [24] Y. P. Malakyan, S. M. Rochester, D. Budker, D. F. Kimball, and V. V. Yashchuk, *Phys. Rev. A* 69 (1), 013817 (2004).
- [25] R. Dicke, *Phys. Rev.* 89, 472 (1953).
- [26] J. Vanier and C. Audoin, *The quantum physics of atomic frequency standards* (A. Hilger, Bristol ; Philadelphia, 1989).
- [27] E. B. Aleksandrov, M. V. Balabas, and V. A. Bonch-Bruyevich, *Pis'ma Zh. Tekh. Fiz.* 13 (11-12), 749 (1987).
- [28] D. Budker, V. Yashchuk, and M. Zolotarev, *Phys. Rev. Lett.* 81 (26), 5788 (1998).
- [29] D. Budker, D. F. Kimball, S. M. Rochester, V. V. Yashchuk, and M. Zolotarev, *Phys. Rev. A* 62 (4), 043403 (2000).
- [30] H. M. Goltenberg, D. Kleppner, and N. F. Ramsey, *Phys. Rev.* 123 (2), 530 (1961).
- [31] C. Rahn and H. G. Robinson, *IEEE J. Quantum Electron.* QE-23 (4), 452 (1987).
- [32] S. Pustelny, D. F. Kimball, V. V. Yashchuk, and D. Budker (2004), to be published.
- [33] F. Grosse, *J. Phys. (Paris)* 29 (5-6), 456 (1968).
- [34] W. Happer, *Rev. Mod. Phys.* 44 (2), 169 (1972).
- [35] R. Jochemsen, M. Morrow, A. J. Berlinsky, and W. N. Hardy, *Phys. Rev. Lett.* 47 (12), 852 (1981).
- [36] A. I. Okunevich, S. M. Rochester, D. Budker, and V. V. Yashchuk (2003), unpublished. Indirect evidence that electron-spin-randomization collisions are significant comes also from an experimental comparison of relaxation rates for the quadrupole and hexadecapole moments for the case of  $^{87}\text{Rb}$  in a paraffin-coated cell similar to the Alle-10 cell, see V. V. Yashchuk, D. Budker, W. Gawlik, D. F. Kimball, Yu. P. Malakyan, and S. M. Rochester, *Phys. Rev. Lett.* 90, 253001 (2003).
- [37] R. Herman and H. M. Mendenhall, *Phys. Rev.* 122, 1204 (1961).
- [38] This cell was kindly loaned to us by Symmetricom, TRC. This does not imply an endorsement by NIST; cells from other companies may work equally well.
- [39] This neglects possible effects of the different mass of the two isotopes. The proportionality of the phase shift and the hyperfine frequency arises from the fact that the mechanism through which the phase shift occurs is the change of the valence-electron density near the nucleus during a collision [30, 37]. This scaling is confirmed, at least approximately, by the present work (see the data for the two Rb isotopes simultaneously present in the Gib cell listed in Table I), and the earlier work of Ref. [15].
- [40] For example, assuming that the intrinsic coating properties at a certain time after manufacturing were identical for the Alle-10 and the Gib cell, we can roughly estimate the temporal drift of the microwave frequency shift as being  $\sim 10\text{ Hz}/30\text{ years}$ .